The Canadian Mineralogist
Vol. 51, pp. 475-494 (2013)
DOI: 10.3749/canmin.51.3.475

LEAD-ANTIMONY SULFOSALTS FROM TUSCANY (ITALY). XIII. PROTOCHABOURNÉITE, ~ $Tl_2Pb(Sb_{9-8}As_{1-2})_{\Sigma 10}S_{17}$, FROM THE MONTE ARSICCIO MINE: OCCURRENCE, CRYSTAL STRUCTURE AND RELATIONSHIP WITH CHABOURNÉITE

PAOLO ORLANDI[§] AND CRISTIAN BIAGIONI

Dipartimento di Scienze della Terra, Università di Pisa, Via S. Maria 53, I-56126 Pisa, Italy

YVES MOËLO

Institut des Matériaux Jean Rouxel, UMR 6502, CNRS, Université de Nantes, 2, rue de la Houssinière, 44 322 Nantes Cedex 3, France

ELENA BONACCORSI

Dipartimento di Scienze della Terra, Università di Pisa, Via S. Maria 53, I-56126 Pisa, Italy

WERNER H. PAAR

Department of Materials Engineering and Physics (Division of Mineralogy), University of Salzburg, Hellbrunnerstrasse 34, A-5020 Salzburg, Austria

ABSTRACT

The new mineral species protochabournéite, ~ $Tl_2Pb(Sb_{9-8}As_{1-2})_{\Sigma 10}S_{17}$, has been discovered in the barite + pyrite + iron oxide ore deposit exploited at the Monte Arsiccio mine, near Sant'Anna di Stazzema (Apuan Alps, Tuscany, Italy). It occurs as compact masses associated with barite, boscardinite, calcite, cymrite, dolomite, pyrite, realgar, routhierite, sphalerite, and stibnite. Protochabournéite is metallic black. Minimum and maximum reflectance data for COM wavelength are [λ (nm): R_{air} (%)]: 470: 36.4/39.5; 546: 34.2/36.7; 589: 33.0/35.4; 650: 31.2/33.4. Electron microprobe analyses collected from two different grains gave (wt.%): Tl 16.81(27), Pb 10.65(17), Sb 41.75(17), As 6.59(4), S 23.43(11), total 99.24(36) and Tl 15.05(26), Pb 13.04(32), Sb 45.49(29), As 3.07(4), S 22.77(14), total 99.42(39). On the basis of Σ*Me* = 13 *apfu*, the chemical formulae are $Tl_{1.89}Pb_{1.18}Sb_{7.90}As_{2.03}S_{16.83}$ and $Tl_{1.74}Pb_{1.48}Sb_{8.81}As_{0.97}S_{16.75}$, respectively, in agreement with the general formula $Tl_{2-x}Pb_{1+2x}(Sb_{10-x-y}As_y)S_{17}$ (x = 0.10–0.24; y = 1–2). Protochabournéite is triclinic $P\overline{1}$, with a 8.150(2), b 8.716(2), c 21.579(4) Å, α 85.18(1)°, β 96.94(1)°, γ 88.60(1)°, V 1515.4(6) Å^3, and Z = 2. The main diffraction lines of the powder diagram, corresponding to multiple (*hkl*) indices, are (relative visual intensity): 3.608 (s), 2.824 (s), 2.790 (ms), 2.170 (vs). The crystal structure of protochabournéite has been solved by X-ray single-crystal studies on the basis of 3401 reflections with a final R_1 = 0.044. It agrees with the general features of chabournéite, but with a primitive unit cell, without any visible superstructure. It presents mixed (Tl,Pb), (Pb,Sb), and (Sb,As) sites, together with pure Tl, Pb, and Sb sites. The structure is composed of two kinds of layers. The first one, derived from the SnS archetype, is closely related to sartorite and parapierrotite, whereas the second one is derived from the PbS archetype. The high Sb:As atomic ratio of protochabournéite appears as the main factor precluding the 2a × 2c superstructure visible in chabournéite as well as in dalnegroite. Protochabournéite, like dalnegroite, belongs to the chabournéite homeotypic series.

Keywords: protochabournéite, new mineral species, sulfosalt, thallium, lead, antimony, arsenic, crystal structure, chabournéite series, Monte Arsiccio mine, Apuan Alps, Tuscany, Italy

§ *E-mail address*: paoloorlandi.pisa@gmail.com

Introduction

During the last thirty years, several new lead-antimony sulfosalts have been discovered in small ore deposits from Apuan Alps, Tuscany, Italy. Among these deposits, the barite-pyrite-iron oxides deposit of the Buca della Vena mine had been the most prolific locality, due to the occurrence of oxysulfosalts (scainiite, Orlandi *et al*. 1999; rouxelite, Orlandi *et al*. 2005) and oxy-chlorosulfosalts (pillaite, Orlandi *et al*. 2001; pellouxite, Orlandi *et al*. 2004). Ore deposits similar to that of Buca della Vena located in the Southern Apuan Alps have been, to date, neglected by mineralogists. However, new and recently collected data allowed identification of rare and sometimes new mineral species, among which are some lead-antimony sulfosalts, *i.e*., parasterryite from the Pollone mine (Moëlo *et al*. 2011) and boscardinite from the Monte Arsiccio mine (Orlandi *et al*. 2012). In particular, the latter locality has shown a very complex sulfosalt assemblage with the occurrence of some very rare minerals and, for the first time in Italy, the presence of thallium sulfosalts. Among these sulfosalts, a chabournéite-like mineral was identified and briefly described by Bonaccorsi *et al*. (2010).

The purpose of this paper is the description of this chabournéite-like mineral as a new lead-thallium-antimony-arsenic sulfosalt species, protochabournéite. The mineral and its name have been approved by the CNMNC-IMA, under the number 2011-054. The holotype specimen of protochabournéite is deposited in the mineralogical collection of the Museo di Storia Naturale, Università di Pisa, Via Roma 79, Calci, Pisa, Italy, with catalogue number 19413. The name emphasizes the close similarity with chabournéite; the prefix "*proto*" (= primary) aims to indicate that this derivative of chabournéite has a primitive unit cell (*i.e*., subcell of chabournéite).

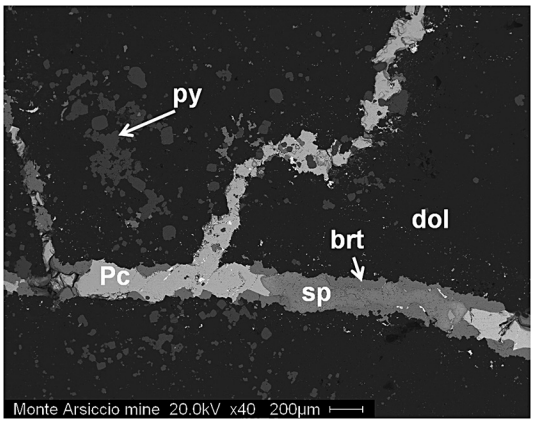

FIG. 1. Protochabournéite vein (Pc) with pyrite (py), barite (brt), and Hg-rich sphalerite (sp), embedded in dolostone (dol; dark grey). The small inclusions in protochabournéite (white in color) are an unidentified Tl–Sb–S phase.

Geological setting

The deposit of barite-pyrite-iron oxides at Monte Arsiccio (latitude 43°58'N, longitude 10°17'E) is located in the Southern Apuan Alps and, in particular, in the northeastern sector of the Sant'Anna tectonic window. In this area, metamorphic rocks belonging to the Apuane and Fornovolasco-Panie units crop out through the non-metamorphic sedimentary formations belonging to the Tuscan Nappe.

The ore deposit exploited in the Monte Arsiccio mine forms an almost conformable lens, with pyrite + barite at the bottom, and iron oxides (magnetite and hematite) + barite at the top, with accessory sulfides and sulfosalts (Carmignani *et al*. 1976, Costagliola *et al*. 1990). The ore is hosted at the contact between phyllites of the *Scisti di Fornovolasco* formation, belonging to the Fornovolasco-Panie Unit and probably related to the Paleozoic basement of the Apuane Unit (Pandeli *et al*. 2004), and Triassic dolostones of the *Grezzoni* formation.

Carmignani *et al*. (1972, 1976) considered the Monte Arsiccio deposit as the product of metasomatic replacement of carbonate rocks, genetically linked to a hypothetical synkinematic intrusive body; however, no field evidence for the occurrence of Tertiary magmatism have been found in the Apuan Alps. Costagliola *et al*. (1990) put forward a different genetic model. According to them, the deposit was formed as a primary Triassic sedimentary-diagenetic proto-ore, which was subsequently metamorphosed and remobilized during the Tertiary Alpine orogeny. In fact, the ore shows conclusive signs of metamorphic deformation and recrystallization, both at macro- and microscopic scales.

Occurrence and Mineral Description

Protochabournéite was identified in two samples collected from the Sant'Olga level (520 m a.s.l.). In the holotype specimen, it occurs in quartz-dolomite-barite veins embedded in dolostones, associated with pyrite, realgar, sphalerite, and stibnite. In the two specimens, protochabournéite occurs as black compact masses, up to 1 cm wide. It is brittle, with conchoidal fracture; cleavage is imperfect. The streak is black and the luster is metallic.

New samples (under study) were identified as veinlets (Fig. 1) embedded in pyrite-rich dolostones, and associated with boscardinite, routhierite, Hg-rich sphalerite, stibnite, twinnite, and a still unidentified Tl–Sb–S phase, which appears brighter in back-scattered electron imaging than the surrounding protochabournéite. Anhedral grains of this latter phase were also identified in saccharoidal barite, together with the same phases cited above.

Under reflected light, protochabournéite appears white, with scarce internal reflections, assuming a dark red color along fractures. The pleochroism is very weak, from very pale yellow to very pale blue. The bireflectance is distinct. With crossed polars, the anisotropism is distinct, with rotation tints from blue green to brown. Table 1 and Figure 2 give the reflectance values of protochabournéite determined in air with WTiC as a standard. The reflectance values are greater than that of chabournéite from Jas Roux (Johan *et al*. 1981) but the trend of the spectrum is very similar. On the contrary, dalnegroite, the As-dominant isotype of chabournéite (Nestola *et al*. 2009), shows a different trend of the reflectance spectrum and higher reflectance values.

The Vickers hardness (load: 15 g) is VHN_{15} = 168 kg/mm^2 (average of five measurements), ranging from 146 to 195 kg/mm^2. The density was not determined, owing to the paucity and small size of the material available for the study. The densities calculated on the basis of the chemical compositions of the two studied samples, A and B, are 5.008 and 5.137 g/cm^3, respectively.

Chemical composition

Two fragments of protochabournéite (samples A and B) were analyzed with a CAMEBAX SX50 electron microprobe (BRGM-CNRS-University common laboratory, Orléans, France). The operating conditions were: accelerating voltage 20 kV; beam current 20 nA; beam size 5 μm; standards (element, emission line, counting times for one spot analysis): pyrite (S *K*α, 20 s), stibnite (Sb *L*α, 20 s), AsGa (As *L*α, 30 s), galena (Pb *M*α, 20 s), lorandite (Tl *M*α, 20 s).

The chemical analyses of these fragments are given in Table 2. The chemical formulae were calculated on the basis of Σ*Me* = 13 atoms per formula unit (*apfu*) in accord with the crystal structure study results. The formula of sample A corresponds to $Tl_{1.89}Pb_{1.18}Sb_{7.90}As_{2.03}S_{16.83}$, and the formula of sample B to $Tl_{1.74}Pb_{1.48}Sb_{8.81}As_{0.97}S_{16.75}$. Each of the two groups of analyses appears very homogeneous, and the two structural formulae fit very well to the general

TABLE 1. REFLECTANCE DATA (%) FOR PROTOCHABOURNÉITE IN AIR

λ(nm)	R_{min}	R_{max}
400	35.9	42.1
420	37.1	40.2
440	36.9	40.2
460	36.5	39.5
470	**36.4**	**39.5**
480	36.5	39.3
500	35.4	37.8
520	34.8	37.2
540	34.4	36.8
546	**34.2**	**36.7**
560	34.1	36.4
580	33.4	35.7
589	**33.0**	**35.4**
600	32.8	35.1
620	32.1	34.4
640	31.5	33.7
650	**31.2**	**33.4**
660	30.7	33.2
680	30.3	32.6
700	29.6	31.8

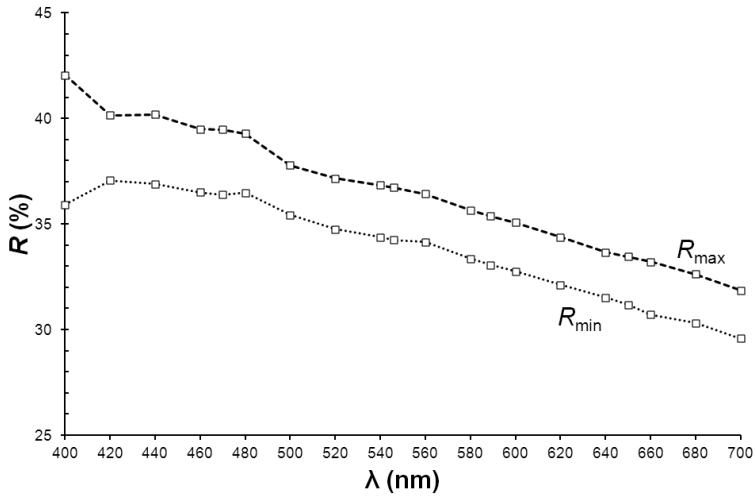

FIG. 2. Reflectance spectra of protochabournéite in air.

formula $Tl_{2-x}Pb_{1+2x}(Sb_{10-x-y}As_y)S_{17}$ (x = 0.10–0.24; y = 1–2), with only a small S deficit. This structural formula is close to half the general formula proposed for chabournéite, $Tl_{5-x}Pb_{2x}(Sb,As)_{21-x}S_{34}$ (Moëlo *et al.* 2008).

Crystallography

The powder X-ray diffraction pattern of protochabournéite from the Monte Arsiccio mine was obtained using a 114.6 mm diameter Gandolfi camera, with Ni-filtered Cu $K\alpha$ radiation. The observed X-ray powder pattern is compared to the calculated one (obtained using the software Powdercell; Kraus & Nolze 1996) in Table 3. The relative intensities of the main measured lines do not fit exactly those of the calculated ones. The discrepancies may be explained as due to the convolution of different peaks. Cell parameters were not refined from the powder-diffraction data because of the multiplicity of indices for the majority of diffraction lines.

Any attempt to find a single crystal suitable for the collection of X-ray diffraction intensity data was unsuccessful. Therefore, a very small fragment was tested at the XRD1 beamline of the Elettra synchrotron radiation facility of Basovizza (Trieste, Italy) and it was found to be composed of two misaligned crystals. A collection of the intensity data was tried, using a wavelength of 1.0 Å. The composite fragment was placed at 36 mm from the 165 mm MarCCD detector; 182 frames were collected, with a rotation angle $\Delta\phi = 2°$. During extraction of the intensity data, it was possible to separate the contributions of the two crystals forming the examined grain. Data were integrated and corrected for Lorentz-polarization and background effects using the Hkl package (Otwinowski & Minor 1997) on the basis of the intensities of equivalent reflections. The cell refinement points to a triclinic unit cell with parameters a 8.150(2), b 8.716(2), c 21.579(4) Å, α 85.18(1), β 96.94(1), γ 88.60(1)°, V 1515.4(6) Å^3.

Notwithstanding the use of a high brilliance radiation such as that of the synchrotron, superstructure reflections along **a** and **c** directions were not observed, contrary to chabournéite, which shows a 16.3 Å periodicity along **a**, and a 42.6 Å c parameter. In this latter sulfosalt, the reflections doubling the c parameter were very weak and, in fact, Nagl (1979) determined the crystal structure of chabournéite in a cell with a halved c. Recently, Bindi *et al.* (2010) confirmed these two superstructures $2a \times 2c$ for dalnegroite, the As-rich derivative of chabournéite. Thus, the unit cell of protochabournéite is a primitive cell corresponding to the subcell of chabournéite and dalnegroite.

The crystal structure was solved through direct methods, using SHELXS-97 (Sheldrick 2008); no systematic absences were observed, indicating a choice of space groups $P1$ or $P\bar{1}$. Although the statistical tests on the distribution of $|E|$ values ($|E^2 - 1| = 0.927$) indicated the possible presence of an inversion center, the crystal structure was initially solved in the space group $P1$, in agreement with the crystal structure of chabournéite given by Nagl (1979). In a first step, the maxima related to (Tl,Pb) atoms were found; successive difference-Fourier maps allowed the introduction of 21 independent Sb and 34 S atoms. The crystal structure refinement converged to $R = 0.053$. A careful examination of the crystal structure revealed the presence of an inversion center. Therefore, atomic coordinates were normalized in the $P\bar{1}$ structure and refined with the program SHELX-97 (Sheldrick 2008). Due to the very similar scattering factors of Pb and Tl, the occupancies of the Tl/Pb sites were fixed initially taking into account the bond distances and the bond-valence balance (Brese & O'Keeffe 1991). Two sites are pure Tl and Pb sites (Tl1 and Pb1 sites, respectively), whereas another (Tl2) is a mixed (Tl,Pb) site, with Tl > Pb. The Sb sites are pure Sb or mixed (Sb,As) sites; the occupancies were refined taking into account the results of the bond-valence balance. The difference-Fourier map suggested the splitting of one Sb site into two sub-positions. As a result, the R value dropped significantly, indicating the presence of a split (Sb,Pb) site, namely the Sb8 and Pb8 sub-sites. The sum of their occupancies was constrained to 1. The refinement converged to $R_1 = 0.0437$ for 3392 reflections with $F_o > 4\sigma(F_o)$, and 0.0438 for all 3401 reflections. Table 4 summarizes the crystal data, and the parameters of the data collection and of the crystal structure refinement. Atomic coordinates, selected bond distances, and bond-valence calculations are reported in Table 5, Table 6, and Table 7, respectively. Figure 3 shows the projection along **b** of the crystal structure

TABLE 2. MICROPROBE ANALYSES OF PROTOCHABOURNÉITE: CHEMICAL COMPOSITION AS WT.% (GIVEN AS ELEMENTS) AND NUMBER OF ATOMS PER FORMULA UNIT (*apfu*) ON THE BASIS OF Σ*Me* = 13 *apfu*

	Sample A	Sample B
Tl (wt.%)	16.81(27)	15.05(26)
Pb	10.65(17)	13.04(32)
Sb	41.75(17)	45.49(29)
As	6.59(4)	3.07(4)
S	23.43(11)	22.77(14)
total	99.24(36)	99.42(39)
Tl (*apfu*)	1.89(3)	1.74(3)
Pb	1.18(2)	1.48(4)
Sb	7.90(5)	8.81(4)
As	2.03(1)	0.97(1)
S	16.83(9)	16.75(10)
Ev*	1.1(5)	1.6(10)
Tl+(Pb/2)	4.97(6)	4.96(4)

* Relative error of the valence equilibrium (%), calculated as [Σ(val+) – Σ(val–)] × 100 / Σ(val–).
* 8 spot analyses for each sample.

TABLE 3. X-RAY POWDER DIFFRACTION DATA FOR PROTOCHABOURNÉITE

I_{obs}	d_{meas}	I_{calc}	d_{calc}	$h\ k\ l$	I_{obs}	d_{meas}	I_{calc}	d_{calc}	$h\ k\ l$
		5	10.67	0 0 2	mw	2.890	44	2.875	2 2 2
		9	7.11	0 0 3			17	2.850	$\bar{2}$ 0 6
		16	6.09	1 0 2			13	2.844	$\bar{1}$ $\bar{2}$ 5
		5	5.816	1 $\bar{1}$ 0			40	2.842	$\bar{2}$ 2 3
		6	5.455	$\bar{1}$ 1 2	**s**	**2.824**	77	2.826	2 $\bar{2}$ 1
		7	5.412	1 $\bar{1}$ 1	**ms**	**2.790**	61	2.804	$\bar{2}$ $\bar{2}$ 3
w	4.73	7	4.668	$\bar{1}$ $\bar{1}$ 3			11	2.769	$\bar{2}$ 0 5
		6	4.377	0 $\bar{1}$ 4			20	2.754	$\bar{1}$ $\bar{1}$ 7
		13	4.328	0 2 1			8	2.747	1 3 1
		14	4.268	0 0 5	m	2.740	39	2.742	2 2 3
mw	4.23	51	4.220	1 0 4			30	2.728	$\bar{2}$ 2 4
mw	4.18	29	4.182	0 $\bar{2}$ 1	m	2.706	25	2.706	2 $\bar{2}$ 2
		7	4.149	0 2 2			13	2.695	3 0 0
vw	4.06	34	4.043	2 0 0			5	2.695	1 3 2
mw	3.959	54	3.982	$\bar{1}$ 0 5			10	2.693	$\bar{3}$ 0 2
mw	3.928	60	3.945	$\bar{2}$ 0 2	mw	2.635	7	2.634	3 0 1
vw	3.850	14	3.858	0 2 3			8	2.631	$\bar{1}$ 0 8
		8	3.806	$\bar{1}$ $\bar{2}$ 1	w	2.606	6	2.606	1 3 3
		13	3.717	$\bar{2}$ 0 3			6	2.592	$\bar{2}$ 0 7
mw	3.673	63	3.670	1 2 2			7	2.588	2 2 4
		18	3.635	2 0 2	w	2.448	20	2.445	1 0 8
		28	3.630	1 $\bar{2}$ 1			8	2.430	1 $\bar{2}$ 6
		46	3.625	$\bar{1}$ 2 2	mw	2.427	10	2.423	3 0 3
s	**3.608**	100	3.596	1 0 5			14	2.420	1 2 7
m	3.554	33	3.568	0 $\bar{2}$ 3			6	2.417	$\bar{3}$ 0 5
		6	3.534	$\bar{1}$ $\bar{1}$ 5	mw	2.394	37	2.398	0 $\bar{2}$ 7
m	3.517	41	3.531	$\bar{1}$ 2 3	m	2.369	49	2.367	0 2 8
		12	3.521	0 2 4			6	2.355	$\bar{1}$ 0 9
		18	3.435	1 2 3	vw	2.331			
m	3.417	40	3.414	$\bar{1}$ 0 6	w	2.289			
		29	3.414	1 $\bar{2}$ 2	w	2.269			
		9	3.380	$\bar{1}$ $\bar{2}$ 3	w	2.233	8	2.229	1 $\bar{2}$ 7
m	3.358	41	3.342	2 0 3	w	2.210			
mw	3.287	27	3.293	$\bar{1}$ 2 4			7	2.180	$\bar{3}$ $\bar{2}$ 4
w	3.135	26	3.134	$\bar{2}$ 0 5	**vs**	**2.170**	14	2.179	$\bar{1}$ $\bar{2}$ 8
		12	3.117	1 0 6			58	2.178	0 4 1
mw	3.095	31	3.110	$\bar{1}$ $\bar{2}$ 4			10	2.170	0 4 0
		5	3.105	$\bar{1}$ $\bar{1}$ 6			5	2.164	0 4 2
		9	3.048	0 0 7			6	2.162	0 2 9
mw	3.045	19	3.046	2 0 4			16	2.155	$\bar{3}$ 0 7
mw	3.025	31	3.033	$\bar{1}$ 2 5	vw	2.141	12	2.140	$\bar{1}$ 2 9
		13	3.011	2 2 0	w	2.025	10	2.025	$\bar{3}$ 0 8
vw	2.969	23	2.976	$\bar{1}$ 0 7	mw	1.994			
		16	2.940	$\bar{2}$ 2 1	mw	1.950			
		25	2.922	$\bar{2}$ $\bar{2}$ 2	mw	1.940			
		7	2.917	$\bar{2}$ 2 2	ms	1.888			
mw	2.903	9	2.908	2 $\bar{2}$ 0	m	1.856			
		8	2.901	1 $\bar{2}$ 4	w	1.828			
		9	2.899	1 2 5					

Notes: the d_{hkl} values were calculated on the basis of the unit cell refined by using single-crystal data. Intensities were calculated on the basis of the structural model; calculated reflections with relative intensities below 5 (over 100) were omitted, if not observed. Observed intensities were visually estimated. vs = very strong; s = strong; ms = medium-strong; m = medium; mw = medium-weak; w = weak; vw = very weak.

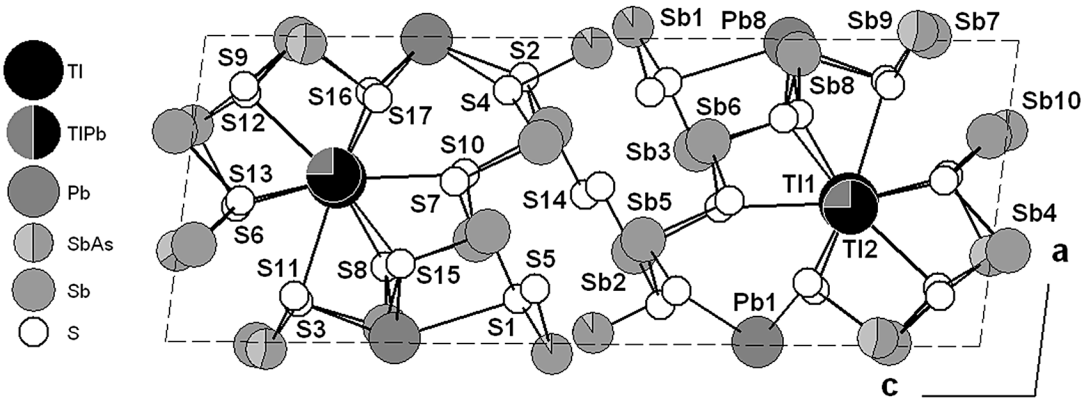

FIG. 3. Projection along **b** of the unit cell of protochabournéite. Atoms in order of decreasing size: Tl (black), Pb (dark grey), Sb (medium grey), (Sb,As) (light grey), and S (white).

TABLE 4. CRYSTAL DATA AND SUMMARY OF PARAMETERS DESCRIBING DATA COLLECTION AND REFINEMENT FOR CHABOURNÉITE

Crystal data	
X-ray formula	$Tl_{1.70}Pb_{1.60}(Sb_{8.80}As_{0.90})_{\Sigma 9.70}S_{17}$
Crystal size (mm^3)	0.25 × 0.20 × 0.15
Cell setting, space group	Triclinic, $P\bar{1}$
a, *b*, *c* (Å);	8.150(2), 8.716(2), 21.579(4);
α, β, γ(°)	85.18(1), 96.94(1), 88.60(1)
V ($Å^3$)	1515.4 (6)
Z	2
Data collection and refinement	
Radiation, wavelength (Å)	synchrotron, λ = 1
Temperature (K)	293
Detector to sample distance	36 mm
Active detection-area (cm^2)	16.5 × 16.5
Number of frames	182
Rotation width per frame (°)	2
Maximum observed 2θ (°)	64.36
Measured reflections	12478
Unique reflections	3401
Reflections $F_o > 4\sigma(F_o)$	3392
R_{int} after absorption correction	0.0443
$R\sigma$	0.0309
Range of *h*, *k*, *l*	$-8 \le h \le 8$, $-9 \le k \le 9$, $-22 \le l \le 22$
R [F_o>4 σ F_o]	0.0437
R (all data)	0.0438
wR (on F_o^2)	0.1229
Goof	1.076
Number of least squares parameters	276
Maximum and minimum residual peak ($e/Å^3$)	1.56 (at 0.82 Å from Pb8) –1.72 (at 0.79 Å from Pb2)

TABLE 5. ATOMIC POSITIONS AND EQUIVALENT DISPLACEMENT PARAMETERS FOR PROTOCHABOURNÉITE

Site	Occupancy	*x*	*y*	*z*	U_{eq} (Å^2)
Tl1	$Tl_{1.00}$	0.4657(1)	0.5978(1)	0.18388(4)	0.0702(4)
Tl2	$Tl_{0.70}Pb_{0.30}$	0.4517(1)	0.0991(1)	0.18031(4)	0.0700(3)
Pb1	$Pb_{1.00}$	0.0101(1)	0.0927(1)	0.27277(3)	0.0584(3)
Sb1	$Sb_{0.90}$ $As_{0.10}$	0.0357(1)	0.7790(1)	0.47663(6)	0.0406(4)
Sb2	$Sb_{1.00}$	0.3007(1)	0.4803(1)	0.43880(5)	0.0367(3)
Sb3	$Sb_{1.00}$	0.6356(1)	0.7776(1)	0.37853(5)	0.0388(4)
Sb4	$Sb_{1.00}$	0.6852(1)	0.1085(1)	0.02106(5)	0.0380(3)
Sb5	$Sb_{1.00}$	0.3425(1)	0.0507(1)	0.42918(5)	0.0408(3)
Sb6	$Sb_{1.00}$	0.6621(1)	0.3067(1)	0.36511(6)	0.0404(3)
Sb7	$Sb_{1.00}$	0.1040(1)	0.3617(1)	0.11215(5)	0.0395(3)
Sb8	$Sb_{0.70}$	0.9473(6)	0.5906(9)	0.2696(3)	0.0465(8)
Pb8	$Pb_{0.30}$	0.9909(11)	0.5962(14)	0.2798(5)	0.0465(8)
Sb9	$Sb_{0.55}As_{0.45}$	0.0263(2)	0.8617(1)	0.12617(6)	0.0395(4)
Sb10	$Sb_{0.65}As_{0.35}$	0.2952(2)	0.3704(1)	–0.00011(5)	0.0380(4)
S1	$S_{1.00}$	–0.1443(4)	0.5812(4)	0.4258(2)	0.0370(9)
S2	$S_{1.00}$	0.1300(5)	0.2526(4)	0.3984(2)	0.0345(9)
S3	$S_{1.00}$	–0.1328(5)	0.6411(5)	0.1571(2)	0.0404(10)
S4	$S_{1.00}$	0.1755(5)	0.8442(4)	0.3806(2)	0.0385(9)
S5	$S_{1.00}$	–0.1791(5)	0.9754(4)	0.4450(2)	0.0429(10)
S6	$S_{1.00}$	0.5576(5)	0.3328(4)	0.0663(2)	0.0390(10)
S7	$S_{1.00}$	0.4724(5)	0.1027(4)	0.3296(2)	0.0388(9)
S8	$S_{1.00}$	0.7524(5)	0.3587(5)	0.2590(2)	0.0428(10)
S9	$S_{1.00}$	0.1651(5)	0.1638(4)	0.0567(2)	0.0437(10)
S10	$S_{1.00}$	0.4475(5)	0.5196(4)	0.3411(2)	0.0350(9)
S11	$S_{1.00}$	–0.1500(5)	0.0649(4)	0.1515(2)	0.0379(9)
S12	$S_{1.00}$	0.1895(5)	0.5615(4)	0.0606(2)	0.0415(10)
S13	$S_{1.00}$	0.5401(5)	0.8907(4)	0.0700(2)	0.0388(9)
S14	$S_{1.00}$	0.5124(4)	0.3016(4)	0.4914(2)	0.0356(9)
S15	$S_{1.00}$	0.7414(5)	0.8113(5)	0.2770(2)	0.0413(10)
S16	$S_{1.00}$	0.1832(5)	0.3322(4)	0.2120(2)	0.0406(10)
S17	$S_{1.00}$	0.2029(6)	0.8470(5)	0.2215(2)	0.0539(12)

of protochabournéite. A cif file is available from the Depository of Unpublished Data of the MAC website [document Protochabournéite CM51_475].

Crystal structure description

Cation coordination and site occupancies

The crystal structure of protochabournéite shows the presence of three large cation sites, a split (Sb8,Pb8) site, nine (Sb,As) sites, and 17 S sites (Fig. 3).

Tl1 is a pure thallium site; it has a triangular prismatic coordination, with three capping ligands. The average bond length is 3.417 Å. Pb1 is a pure lead site, showing a bicapped triangular prismatic coordination, with an average bond length of 3.160 Å. The third large cation site Tl2 is a mixed (Tl,Pb) site; it shows a tricapped triangular prismatic coordination, with an average bond length of 3.355 Å, in agreement with the partial substitution of thallium by lead. Its site occupancy was fixed to ($Tl_{0.70}Pb_{0.30}$), in order to maintain the charge equilibrium due to the coupled substitution $Tl^+ + Sb^{3+} = 2\ Pb^{2+}$, with an equal amount of Pb entering the Tl2 and (Sb8,Pb8) sites. The latter is a split site, with two sub-positions at a distance of 0.38 Å. Considering only the distances shorter than 3 Å, Sb8 is a three-fold coordinated Sb atom. Pb8 is a monocapped trigonal prism, with two very long additional bonds. The refined occupancy pointed to $Sb_{0.69}Pb_{0.31}$; it was then fixed to $Sb_{0.70}Pb_{0.30}$. This pair (Sb8,Pb8) alternates along [010] with the Pb1 site.

Among the ten (Sb,As) sites, pure Sb sites are Sb2 to Sb7, whereas Sb1, Sb9, and Sb10 are mixed (Sb,As) sites. Their occupancies were refined considering the results of the bond-valence calculations (Table 7). Sb1 is the As-poorest mixed site (10 at.% As), whereas the two other mixed sites, namely Sb9 and Sb10, are richer in As (45 and 35 at.%, respectively). Taking into account only the (Sb,As)–S distances shorter than ~ 2.70 Å, all these (Sb/As) sites are pyramidal three-fold coordinated, with an average bond length varying from 2.395 Å for Sb9 (the As-richest site) to 2.556 Å for the Sb3 site.

TABLE 6. SELECTED BOND DISTANCES (IN Å) IN PROTOCHABOURNÉITE

Tl1– S17	3.234(4)	Tl2– S16	3.124(4)	Pb1– S11	2.812(4)	Sb1– S5	2.414(4)
– S8	3.273(4)	– S17	3.172(6)	– S16	2.864(4)	– S4	2.514(4)
– S12	3.312(4)	– S7	3.209(4)	– S17	2.988(4)	– S1	2.526(4)
– S16	3.375(4)	– S13	3.249(4)	– S8	3.061(4)	– S5	3.009(4)
– S3	3.415(5)	– S6	3.271(4)	– S4	3.190(4)	– S2	3.153(4)
– S10	3.425(4)	– S9	3.327(4)	– S2	3.211(4)	– S1	3.658(4)
– S15	3.506(4)	– S11	3.388(4)	– S15	3.330(5)	– S14	3.702(4)
– S13	3.507(4)	– S15	3.723(4)	– S7	3.824(4)		
– S6	3.700(4)	– S8	3.731(4)				
Sb2– S14	2.407(4)	Sb3– S15	2.448(4)	Sb4– S13	2.488(4)	Sb5– S2	2.432(4)
– S10	2.551(4)	– S1	2.511(4)	– S6	2.515(4)	– S4	2.508(4)
– S2	2.601(4)	– S5	2.708(4)	– S13	2.522(4)	– S7	2.519(4)
– S14	2.876(4)	– S10	2.867(4)	– S11	2.958(4)	– S14	2.948(4)
– S1	3.335(4)	– S7	3.144(4)	– S9	3.310(4)	– S5	3.158(5)
– S4	3.397(4)	– S14	3.217(4)	– S12	3.486(4)	– S14	3.495(4)
– S1	3.682(4)	– S4	3.787(4)	– S9	3.943(4)	– S5	3.906(4)
Sb6– S7	2.493(4)	Sb7– S16	2.418(4)	Sb8– S3	2.436(8)	Pb8– S3	2.710(10)
– S10	2.496(4)	– S12	2.567(4)	– S15	2.549(8)	– S15	2.723(12)
– S8	2.498(4)	– S9	2.569(4)	– S8	2.610(8)	– S8	2.900(11)
– S14	3.114(4)	– S3	2.961(4)	– S17	3.281(9)	– S17	3.097(14)
– S1	3.184(4)	– S11	3.031(4)	– S16	3.339(9)	– S16	3.292(13)
– S5	3.381(4)	– S6	3.724(4)	– S1	3.534(9)	– S4	3.438(10)
– S2	3.804(4)	– S12	3.881(4)	– S4	3.754(6)	– S1	3.454(13)
						– S10	3.819(8)
Sb9– S17	2.357(4)	Sb10– S12	2.409(4)			– S2	3.828(13)
– S11	2.394(4)	– S6	2.425(4)				
– S3	2.437(5)	– S9	2.430(5)				
– S9	3.218(5)	– S6	3.181(4)				
– S12	3.394(4)	– S13	3.190(4)				
		– S3	3.495(4)				

TABLE 7. BOND VALENCE BALANCE CALCULATIONS ACCORDING TO BRESE & O'KEEFFE (1991)

	Tl1	Tl2*	Pb	Sb1*	Sb2	Sb3	Sb4	Sb5	Sb6	Sb7	Sb8*	Pb8*	Sb9*	Sb10	Σ anions
S1				0.85	0.13	0.85			0.14		0.04	0.03			2.04
S2			0.17	0.14	0.66			1.06	0.03			0.01			2.07
S3	0.12									0.25	0.73	0.19	0.85	0.05	2.19
S4			0.18	0.78	0.08	0.03		0.85			0.02	0.03			1.97
S5				1.27		0.50		0.17	0.08						2.02
S6	0.06	0.17					0.84			0.03				1.04	2.14
S7		0.20	0.03			0.15		0.83	0.89						2.10
S8	0.18	0.05	0.25						0.88		0.45	0.12			1.93
S9		0.14					0.12			0.72			0.10	0.91	1.99
S10	0.12				0.76	0.32			0.88			0.01			2.09
S11		0.12	0.49				0.25			0.21			0.95		2.02
S12	0.16						0.06			0.75			0.06	0.96	1.99
S13	0.09	0.18					1.72							0.12	2.11
S14				0.03	1.44	0.13		0.32	0.17						2.09
S15	0.09	0.05	0.12			1.01					0.54	0.19			2.00
S16	0.13	0.25	0.43							1.09	0.06	0.04			2.00
S17	0.20	0.22	0.31								0.07	0.07	1.05		1.92
Σ cations	1.15	1.38	1.98	3.07	3.07	2.99	2.99	3.23	3.07	3.05	1.91	0.69	3.01	3.08	

* Bond valences calculated according to the s.o.f. of each cation in mixed or split sites.

General organization according to modular analysis

Figure 4 is an enlarged projection along **b** of the crystal structure of protochabournéite. This crystal structure agrees with the general features given by Nagl (1979) for chabournéite from Jas Roux, but on the basis of a simpler, more symmetric unit cell ($P\bar{1}$ instead of $P1$), without any visible superstructure. Whereas in Nagl (1979), all cation positions correspond to pure Tl, Pb, Sb, or As sites, this new structure presents mixed (Tl,Pb), (Sb,Pb), and (Sb,As) sites, together with pure Tl, Pb, and Sb sites.

In accordance with Makovicky (1985), the crystal structure of protochabournéite can be described as formed of two kinds of slabs (Fig. 4). The first one ("thin slab", ***t***) derives from the SnS archetype (projection along **b** corresponding to projection on $(010)_{SnS}$ (Del Bucchia *et al*. 1981) and is closely related to sartorite (Berlepsch *et al*. 2003) and parapierrotite (Engel 1980). The second one ("thick slab", ***T***) is of the PbS archetype. Weak bonding in the middle plane of this last slab may act as a cleavage plane (tie-line in Fig. 4).

The inner part of the ***T*** slab can be described as a rod-layer. In the classification of Makovicky (1993), this rod-layer belongs to the Type-2, with jamesonite as the chief member. Figure 5 compares these two rod-layers and a third one corresponding to synthetic $Ca_{0.76}In_{2.84}S_5$ (Eisenmann & Hofmann 1991). In each structure, the building rod is defined by (1) its width (number N of coordination pyramids) and (2) its thickness (number N' of atomic layers). One has N = 3, N' = 4 for jamesonite, $FePb_4Sb_6S_{14}$; N = 3, N' = 3 for $Ca_{0.76}In_{2.84}S_5$ [or $(Ca_{1.52}\square_{0.48})_{\Sigma 2}(In_{5.68}\square_{0.32})_{\Sigma 6}S_{10}$]; and N = 2, N' = 3 for the rod-layer $Sb_3(Sb,As)_2S_7$ of protochabournéite.

Among pure Sb sites, Sb2, Sb3, Sb5, and Sb6 are located in the ***T*** slab, whereas Sb4 and Sb7 are located in the ***t*** slab. Among (Sb,As) sites, Sb1 is located in the

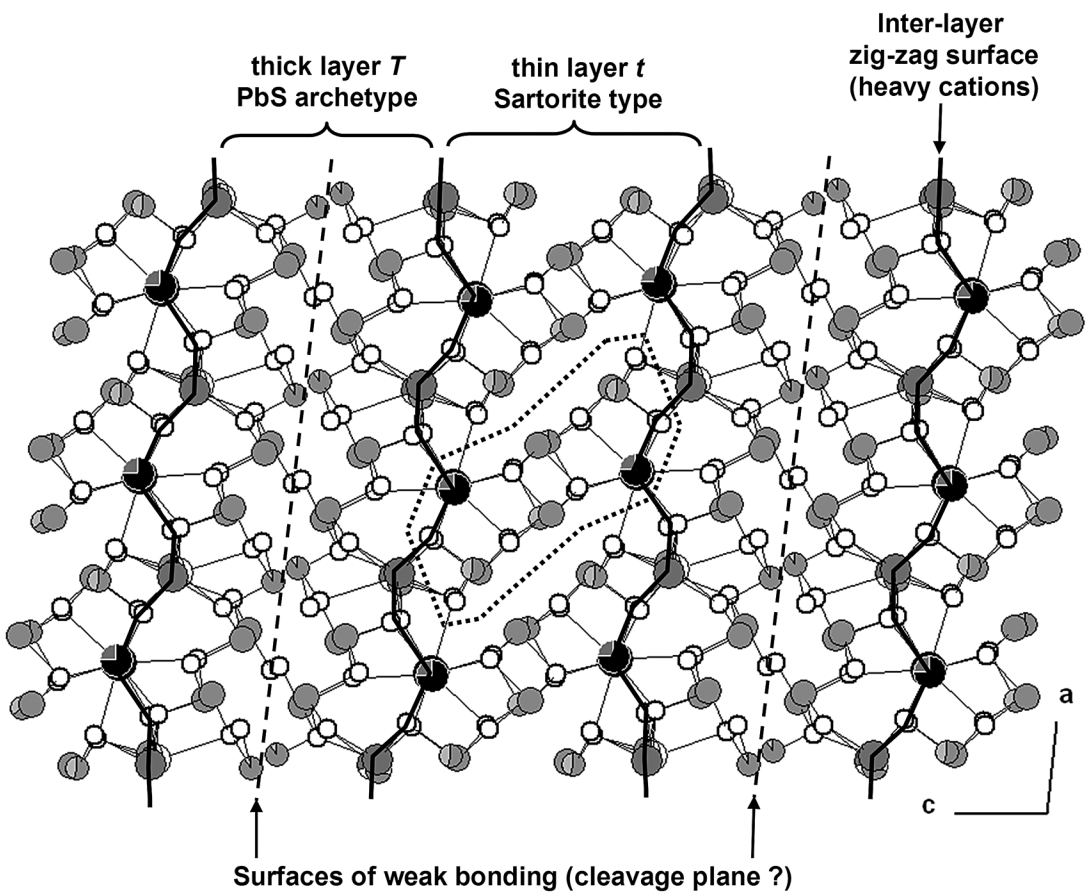

FIG. 4. Enlarged projection along **b** of the crystal structure of protochabournéite, showing its layered organization (thin ***t*** and large ***T*** layers). The dotted line within the thin layer indicates the sartorite-type ribbon.

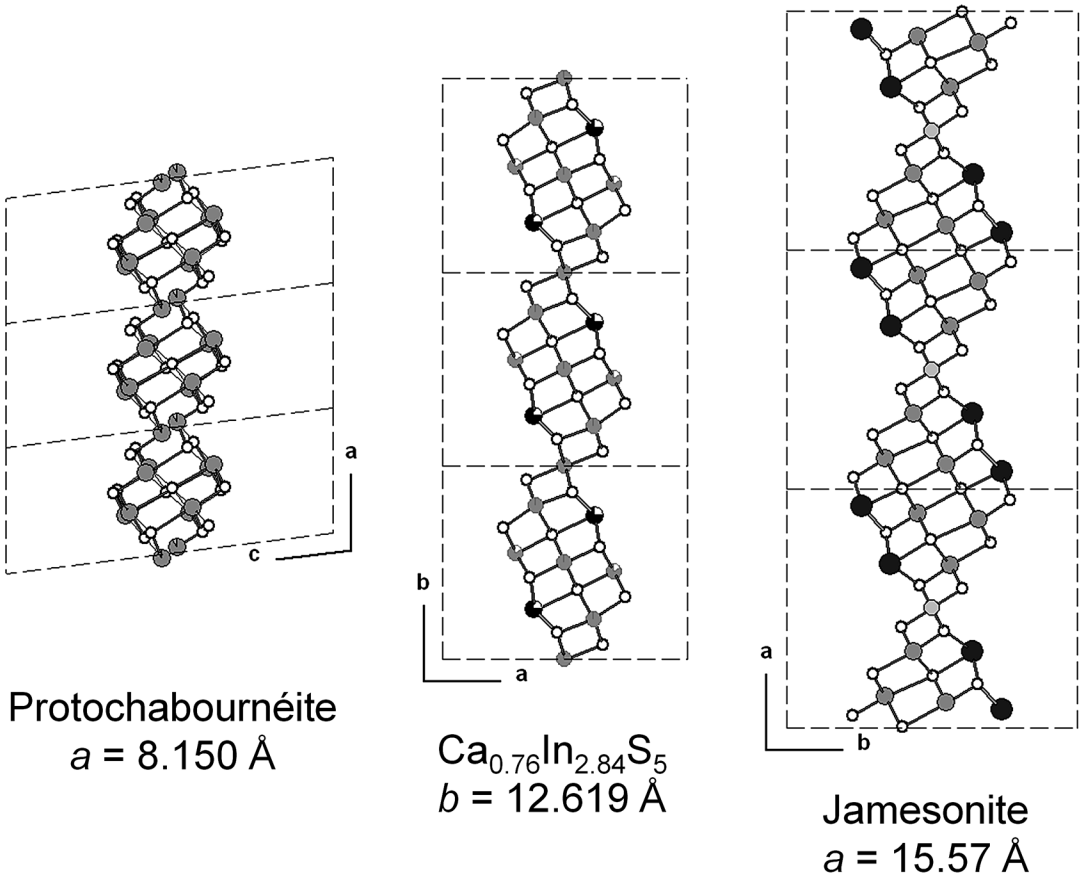

FIG. 5. Comparison of the inner rod-layer of the ***T*** slab of protochabournéite to the constitutive rod-layers of $Ca_{0.76}In_{2.84}S_5$ and jamesonite.

T slab, whereas Sb9 and Sb10 are located in the ***t*** slab, which thus appears enriched in As relative to the ***T*** slab.

Polymerization of (Sb/As) sites

Within the slabs, the examination of the sub-organization of (Sb,As) sites, taking into account only the shortest (Sb,As)–S bonds, permits revelation of their polymeric organization into finite $(Sb,As)_mS_n$ groups. As exemplified by Moëlo *et al.* (2012), only (Sb,As)–S bonds below 2.70 Å (*i.e.*, corresponding to a Sb–S bond valence above 0.5 valence unit) have been selected. Thus, $(Sb,As)S_3$ triangular pyramidal polyhedra appear, and their interconnection forms finite $(Sb,As)_mS_n$ polymers.

In the ***t*** layer, Figure 6 represents the selection of one oblique ribbon (of the sartorite type, see Fig. 4) projected sub-parallel to **b**. As observed in other phases characterized by the occurrence of sartorite-type layers, protochabournéite shows a central polymer, here $[Sb_4(Sb,As)_2]_{\Sigma6}S_{10}$, with two lateral $(Sb,As)S_3$ groups (corresponding to the Sb9 position). Such a polymeric organization has also been described in the other thallium-lead antimony sulfosalt from Monte Arsiccio, boscardinite (Orlandi *et al.* 2012), with the polymer $[Sb_4(As_{0.745}Sb_{0.255})_2]_{\Sigma6}S_{10}$ flanked by two $(Sb_{0.71}As_{0.29})S_3$ groups. In the crystal structure of chabournéite from Jas Roux (Nagl 1979), these oblique ribbons have the composition $(AsS_3)_2[Sb_4As_2]_{\Sigma6}S_{10}$. In the crystal structure of dalnegroite (Bindi *et al.* 2010), a similar topological arrangement of the ***t*** layer is probably present, but Sb and As atoms do not show the triangular pyramidal coordination, probably due to limitations of the diffraction data and refinement.

In the ***T*** layer, it is also possible to discriminate $[Sb_4(Sb,As)]_{\Sigma5}S_9$ polymers (Fig. 7), which are separated by the (Sb8,Pb8) split site. If one considers, for instance, this (Sb8,Pb8) split site in the ideal 2:1 ratio, and the

regular alternation of two Sb8 with one Pb8, these two Sb8 (1) are connected with two Sb9 of the ***t*** layer, and (2) connect three $[Sb_4(Sb,As)]_{\Sigma5}S_9$ polymers. The result is a complex polymer, $[Sb_{14}(Sb,As)_5]_{\Sigma19}S_{33}$. This polymer is oriented along [110] of protochabournéite, and corresponds to the [210] direction of the PbS archetype (Fig. 8).

Along [101] of chabournéite from Jas Roux (Nagl 1979), $(As_3Sb_2)_{\Sigma5}S_9$ polymers alternate with $(Sb_3As_2)_{\Sigma5}S_9$, whereas in protochabournéite there is only one type of $[Sb_4(Sb,As)]_{\Sigma5}S_9$ polymer. This may be the cause of the doubling of the *a* parameter in chabournéite.

Crystal chemistry

Structural formula

The crystal-chemical formula of protochabournéite, as obtained through the refinement of the crystal structure, is $Tl_{1.70}Pb_{1.60}(Sb_{8.80}As_{0.90})_{\Sigma9.70}S_{17}$, in agreement with the results of the chemical analysis of sample B. Doubling this structural formula agrees with the general formula $Tl_{5-x}Pb_{2x}(Sb,As)_{21-x}S_{34}$ proposed for chabournéite, with $x \sim 1.6$.

The two slabs ***t*** and ***T*** observed in the crystal structure of protochabournéite present distinct chemical compositions. The mono-atomic zig-zag surface with

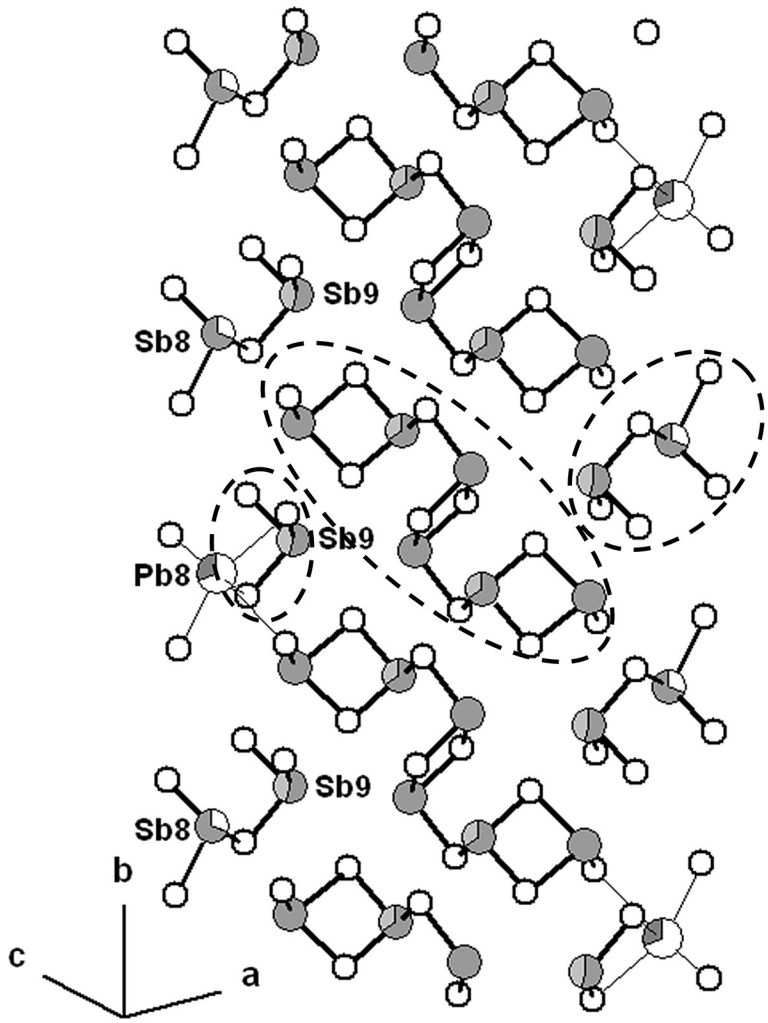

FIG. 6. Polymeric organization of the (Sb,As) atoms with S atoms (short bonds) in the ***t*** slab.

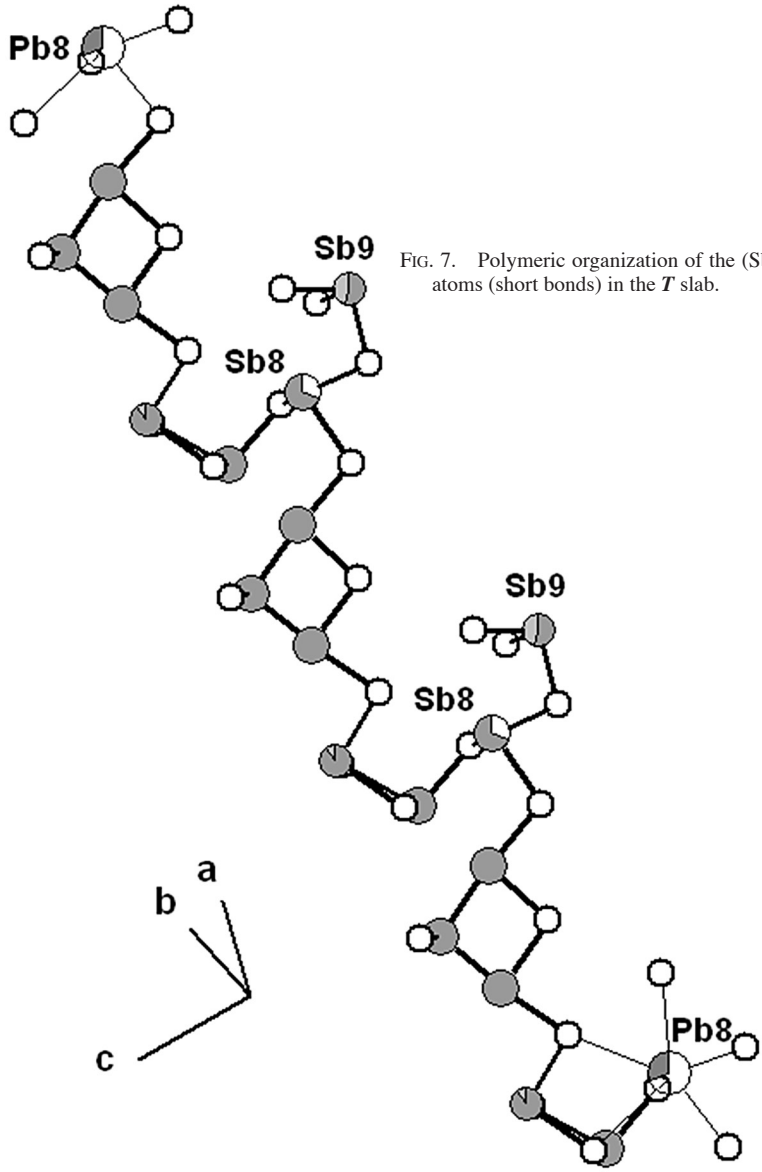

FIG. 7. Polymeric organization of the (Sb,As) atoms with S atoms (short bonds) in the ***T*** slab.

heavy atoms common to these slabs (see Fig. 4) has the composition $Tl(Tl_{0.7}Pb_{0.3})Pb(Pb_{0.3}Sb_{0.7})S_4$ (1).

The composition of the ***t*** slab is obtained by adding formula (1) to the atoms between the zig-zag surfaces:

$$Tl(Tl_{0.7}Pb_{0.3})Pb(Pb_{0.3}Sb_{0.7})S_4 + Sb_{6.4}As_{1.6}S_{12} = Tl_{1.7}Pb_{1.6}Sb_{7.1}As_{1.6}S_{16},$$

or $$(Tl_{1.7}Pb_{1.6}Sb_{0.7})_{\Sigma 4}(Sb_{6.4}As_{1.6})_{\Sigma 8}S_{16} \quad (2).$$

Similarly, the ***T*** slab has the composition:

$$Tl(Tl_{0.7}Pb_{0.3})Pb(Pb_{0.3}Sb_{0.7})S_4 + Sb_{9.8}As_{0.2}S_{14} = Tl_{1.7}Pb_{1.6}Sb_{10.5}As_{0.2}S_{16},$$

or $$(Tl_{1.7}Pb_{1.6}Sb_{0.7})_{\Sigma 4}(Sb_{9.8}As_{0.2})_{\Sigma 10}S_{18} \quad (3).$$

In formula (2), one positive charge is lacking, whereas one negative charge is lacking in (3); the whole formula is therefore charge-balanced.

Comparison of formulas (2) and (3) shows that the inner part of the ***t*** slab concentrates As relatively to the inner part of the ***T*** slab, with $As/(Sb + As)_{at.}$ equal to 0.2

and 0.02, respectively. Arsenic is absent in the common mono-atomic zig-zag surface.

According to its formula, the ***t*** slab is chemically closer to parapierrotite, $TlSb_5S_8 \times 2 = (Tl_2Sb_2)_{\Sigma4}Sb_8S_{16}$, than to sartorite. Formula (3) of the ***T*** slab is similar to that of hutchinsonite, $TlPbAs_5S_9 \times 2 = Tl_2Pb_2As_{10}S_{18}$, but the structure of hutchinsonite is quite different (Matsushita & Takéuchi 1994).

Comparison to chabournéite and dalnegroite

Figure 9 compares the chemical data for protochabournéite to those published for chabournéite (Mantienne 1974, Johan *et al*. 1981, Shimizu *et al*. 1999) and its As-dominant derivative dalnegroite (Bindi *et al*. 2010), on the basis of the Sb/(Sb + As) *versus* Pb/(Pb + 2Tl) atomic ratios (R_{Sb} and R_{Pb}, respectively). This second ratio R_{Pb} corresponds to the heterovalent substitution $Sb^{3+} + Tl^{+} \rightarrow 2\ Pb^{2+}$. All three species are clearly discriminated by their R_{Sb} ratio: around 0.40 for dalnegroite, between 0.50 and 0.60 for chabournéite, and between 0.80 and 0.90 for protochabournéite. The two samples from Monte Arsiccio show a very high Pb content, corresponding to $R_{Pb} = 0.24$ (sample A) and 0.30 (sample B). Generally, chabournéite has a lower Pb content, with R_{Pb} ranging from 0.23 down to 0, whereas in dalnegroite R_{Pb} it is between 0.16 and 0.24.

Another very probable occurrence of chabournéite is the Hemlo gold deposit (Ontario, Canada), where Harris (1989) described a sulfosalt with the composition $Tl_5Pb_2(Sb,As)_{24}S_{43}$, closely associated with pyrite in a routhierite-bearing sample. Donald C. Harris did not publish his finding, but released to one of us (Y.M.) the microprobe analysis; the chemical composition gives $R_{Sb} = 0.54$ and $R_{Pb} = 0.17$, quite within the composition field of chabournéite (Fig. 9).

One analysis of "chabournéite" from the Toya-Takarada mine (Abuta-gun, Japan) presents an anomalous composition, with $R_{Sb} = 0.48$ and high excess Pb ($R_{Pb} = 0.42$). Without crystal structure data, it is not possible to relate this compound to dalnegroite, chabournéite, or a new structural derivative. It will be given a provisory name, "Pb-excess chabournéite derivative".

In the crystal structure of chabournéite (Nagl 1979), the ***t*** slab has the composition $(Tl_4Pb_2Sb_2)_{\Sigma8}(Sb_8As_8)_{\Sigma16}S_{32}$ and the ***T*** slab has the composition $(Tl_4Pb_2Sb_2)_{\Sigma8}(Sb_9As_{11})_{\Sigma20}S_{36}$. This crystal structure shows a slightly higher As/Sb ratio in the inner part of the ***T*** slab, with As more abundant than Sb. This partitioning is the opposite of that observed in protochabournéite from Monte Arsiccio. Nevertheless, the true cation partitioning in Nagl's structure is probably more complicated, as pointed out by Makovicky (1985). Calculation of bond-

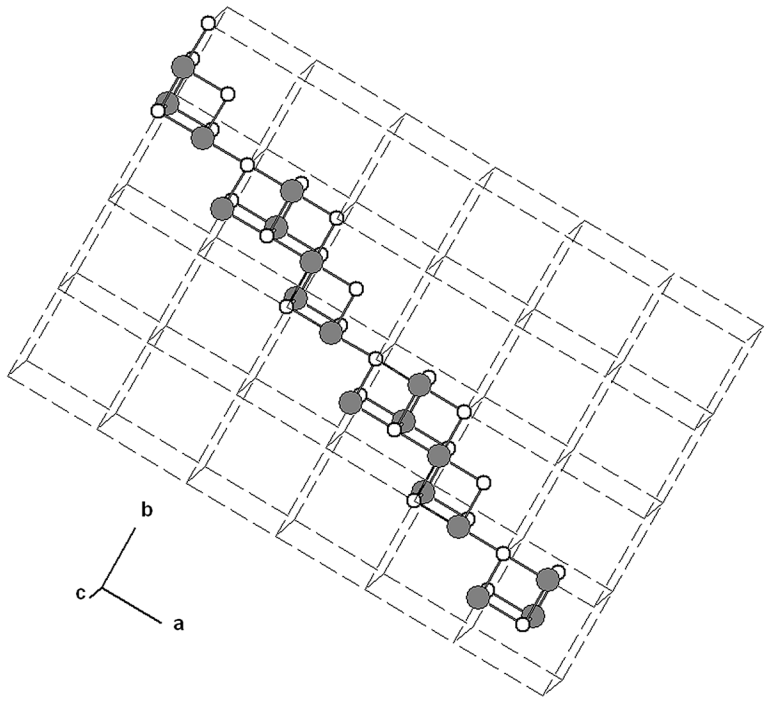

FIG. 8. Selection along the [210] direction of the PbS structure of a (Pb,S) polymeric chain as the basis for the polymeric organization in the ***T*** slab of protochabournéite.

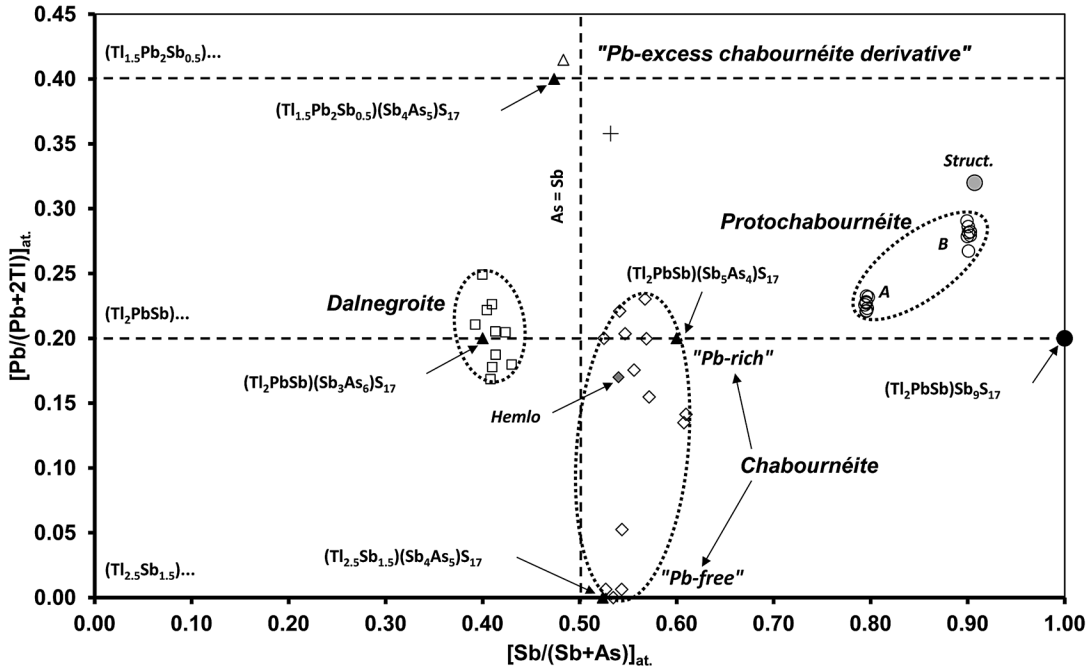

FIG. 9. Pb/(Pb + 2Tl) *versus* Sb/(Sb + As) atomic ratio in the chabournéite series. Open squares: dalnegroite (Nestola *et al.* 2009). Open lozenges: chabournéite from Jas Roux (Mantienne 1974, Johan *et al.* 1981) and Abuta (Shimizu *et al.* 1999). Grey lozenge: chabournéite from Hemlo (D. Harris, writ. commun. 1989). Open triangle: Pb-excess chabournéite from Abuta (Johan *et al.* 1981). Open circles: protochabournéite (this study). Grey circle: chemical composition of protochabournéite on the basis of crystal structure study. Cross: proposed chemical composition of chabournéite studied by Nagl (1979) on the basis of BVS (see Table 8).

valence sum (BVS) for the Sb and As positions shows that many of them are mixed (Sb,As) sites (Table 8): for Sb, when BVS >> 3, and for As, when BVS << 3. Moreover, some Sb sites with BVS << 3 may correspond to mixed (Sb,Pb) sites. While BVS are good for Pb, all BVS for Tl are significantly over 1, indicating mixed (Tl,Pb) sites. In Table 9, a new cation distribution is proposed to adjust the effective bond-valences of these probable mixed sites to the calculated BVS. One obtains the formula $Tl_{6.26}Pb_{6.98}Sb_{20.62}As_{18.14}S_{68}$, with a good charge balance. Nevertheless, whereas the Sb/(Sb + As) ratio is quite in agreement with the formula of Nagl (1979), the Pb/(Pb + Tl) ratio is too high. It is clear that chabournéite from Jas Roux needs a more accurate crystal structure refinement, for a careful comparison with protochabournéite and dalnegroite.

In the very complicated structure of dalnegroite (Bindi *et al.* 2010), the 42 Å periodicity corresponds to the regular alternation of two thick (***T1*** and ***T2***) and two thin (***t1*** and ***t2***) layers (***T1*** → ***t1*** → ***T2*** → ***t2*** sequence), with the compositions ***T1*** – $Tl_4Pb_{2.205}(Sb_{4.43}As_{17.365})_{\Sigma 21.795}S_{36}$; ***t1*** – $Tl_4Pb_{1.54}(Sb_{6.095}As_{12.365})_{\Sigma 18.46}S_{32}$; ***T2*** – $Tl_4Pb_{1.545}(Sb_{11.455}As_{11})_{\Sigma 22.455}S_{36}$; and ***t2*** – $Tl_4Pb_{2.73}(Sb_{9.27}As_8)_{\Sigma 17.27}S_{32}$. Each (***T1***, ***T2***) and (***t1***, ***t2***) pair has opposite Sb/As ratios, and the 21 Å-substructure would give the compositions ***T*** – $Tl_4Pb_{1.875}(Sb_{7.9425}As_{14.1825})_{\Sigma 22.125}S_{36}$, and ***t*** – $Tl_4Pb_{2.135}(Sb_{7.6825}As_{10.1825})_{\Sigma 17.865}S_{32}$, with As/(Sb + As) atomic ratios equal to 0.64 and 0.57, respectively (to be compared with ratios 0.50 and 0.44 for chabournéite from Jas Roux).

DISCUSSION

Protochabournéite: A homeotypic derivative of chabournéite

Initially, protochabournéite from Monte Arsiccio was described as a new occurrence of chabournéite (Bonaccorsi *et al.* 2010). A more careful analysis of the crystal chemistry permitted us to consider it as homeotypic derivative, *i.e.*, a new mineral species with its own name. According to Lima-de-Faria *et al.* (1990), protochabournéite appears as a homeotype of chabournéite because they have (1) the same basic structural scheme (identical topologies), (2) distinct unit

TABLE 8. BOND VALENCE SUM (BVS) FOR CATIONS IN THE CRYSTAL STRUCTURE OF CHABOURNÉITE BY NAGL (1979) AND HYPOTHETICAL DISTRIBUTION INTO MIXED SITES (Tl,Pb), (Pb,Sb) AND (Sb,As) TO ADJUST THE CATION DISTRIBUTION TO BVS

		Proposal				Proposal					Proposal	
	BVS	Tl	Pb		BVS	Pb	Sb	As		BVS	Sb	As
Tl1	1.19	0.85	0.15	Sb1	3.07		1.00		As1	2.55	0.26	0.74
Tl2	1.25	0.80	0.20	Sb2	2.70	0.17	0.83		As2	2.46	0.32	0.68
Tl3	1.44	0.66	0.34	Sb3	3.33		0.75	0.25	As3	2.70	0.17	0.83
Tl4	1.12	0.90	0.10	Sb4	3.02		1.00		As4	2.26	0.49	0.51
Tl5	1.31	0.75	0.25	Sb5	2.52	0.27	0.73		As5	2.38	0.39	0.61
Tl6	1.24	0.80	0.20	Sb6	2.21	0.47	0.53		As6	2.71	0.16	0.84
Tl7	1.30	0.76	0.24	Sb7	3.10		0.92	0.08	As7	2.81	0.10	0.9
Tl8	1.33	0.74	0.26	Sb8	3.15		0.88	0.12	As8	3.04		1.00
Pb1	2.07		1.00	Sb9	2.81	0.10	0.90		As9	3.02		1.00
Pb2	2.06		1.00	Sb10	3.27		0.79	0.21	As10	2.86	0.07	0.93
Pb3	1.98		1.00	Sb11	3.27		0.79	0.21	As11	2.86	0.07	0.93
Pb4	1.90		1.00	Sb12	2.79	0.11	0.89		As12	2.86	0.07	0.93
				Sb13	2.91		1.00		As13	2.93		1.00
				Sb14	3.17		0.86	0.14	As14	3.21		1.00
				Sb15	2.99		1.00		As15	3.05		1.00
				Sb16	2.77	0.12	0.88		As16	2.46	0.33	0.67
				Sb17	3.26		0.80	0.20	As17	2.57	0.25	0.75
				Sb18	3.24		0.82	0.18	As18	2.76	0.13	0.87
				Sb19	3.55		0.61	0.39	As19	2.36	0.41	0.59
				Sb20	3.40		0.71	0.29				
				Sb21	3.40		0.71	0.29				

	Tl	Pb	Sb	As	Val. +	S	Val. -	Pb/(Pb+Tl)	Sb/(Sb+As)
Nagl (1979)	8	4	21	19	136	68	136	0.333	0.525
proposal	6.26	6.98	20.62	18.14	136.5	68	136	0.527	0.532

TABLE 9. CRYSTALLOGRAPHIC PARAMETERS OF THE MEMBERS OF THE CHABOURNÉITE SERIES AND THEIR SITE OF OCCURRENCE

	a (Å)	*b*(Å)	*c* (Å)	α (°)	β (°)	γ (°)	*V* (Å^3) (*V*$_{sub}$)*	Ref.
"Pb-free" chabournéite	16.346	42.602	8.534	95.86	86.91	96.88	5863.5 (1465.9)	[1]
"Pb-rich" chabournéite	16.33	8.53	21.24	93.85	95.40	104.48	2952 (1476)	[2]
chabournéite	16.320	42.636	8.543	83.98	89.06	83.20	5870.17 (1467.54)	[3]
dalnegroite	16.218	42.546	8.558	95.70	90.18	96.38	5838.9 (1459.7)	[4]
protochabournéite	8.150	8.716	21.579	85.18	96.94	88.60	1515.4	[5]

[1] Jas Roux, Hautes-Alps, France (Johan *et al*., 1981); [2] Jas Roux, Hautes-Alps, France (Mantienne, 1974); [3] Jas Roux, Hautes-Alps, France (Nagl, 1979); [4] Lengenbach, Binntal, Switzerland (Nestola *et al*., 2009); [5] Monte Arsiccio mine (this work).

cells [chabournéite (C) is a superstructure of protochabournéite (P): $a_C = 2a_P$, and $b_C = 2c_P$ – Table 9] and space groups [C: *P*1; P: $P\bar{1}$, for the (*a*, *b*/2, *c*) subcell of Nagl, 1979], and (3) distinct chemical compositions related to the occupancy of some sites by distinct atomic species. This last point is the most important to distinguish a homeotype from a polytype (no significant chemical change). While in protochabournéite all (Sb,As) sites have Sb >> As, in chabournéite (Nagl

1979) there is a strong partitioning between Sb sites (21 positions) and As sites (19 positions).

The chabournéite homeotypic series

In dalnegroite, the As-dominant derivative of chabournéite (Nestola *et al.* 2009), there is also a strong partitioning between Sb- and As-dominant sites (Bindi *et al.* 2010). On the basis of all of their crystal chemical characteristics, chabournéite, protochabournéite, and dalnegroite constitute the members of the chabournéite homeotypic series (Table 9), within the sartorite homologous series (Moëlo *et al.* 2008).

A general simplified structural formula can be proposed on the basis of the primitive cell (or subcell) of members of this series, *i.e.*, 13 cations and 17 S atoms: $[Tl_{2-x}Pb_{1+2x}Sb_{1-x}]_{\Sigma4}\bullet(Sb_{9-y}As_y)S_{17}$. The first part of this formula represents the inter-layer atom plane, with the heavy metals. With $x = y = 0$, one has the ideal Sb endmember of the series, with composition $Tl_2PbSb_{10}S_{17}$ (Fig. 9). Protochabournéite is very close to this endmember, with small positive values of x (*i.e.*, slight Pb excess) and y. Note that for x positive, Pb excess replaces Tl and Sb over two distinct sites, whereas for x negative, Tl and Sb replace Pb at the same site.

In analyses of chabournéite from Abuta (Johan *et al.* 1981, Shimizu *et al.* 1999), on the basis of the Pb content with $\Sigma Me = 13$ *apfu*, x values vary between –0.12 and +0.06, and y (equal to the As content) varies from 4.25 up to 4.59. This is close to the stoichiometric formula $[Tl_2PbSb]_{\Sigma4}\bullet(Sb_5As_4)S_{17}$ [or $Tl_2Pb(Sb,As)_{10}S_{17}$, as proposed by Shimizu *et al.* 1999]. At Jas Roux, chabournéite shows a large solid solution field essentially related to the substitution $Sb^{3+} + Tl^+ \rightarrow 2\ Pb^{2+}$. In the first study by Mantienne (1974), the two microprobe analyses are close to $x = –0.13$ and $y = 3.9$. In analyses by Johan *et al.* (1981), x varies from –0.37 down to –0.50 (*i.e.*, Pb absent), and y from 4.82 up to 5.00; it is close to the ideal formula $[Tl_2(Tl_{0.5}Sb_{0.5})Sb]_{\Sigma4}\bullet(Sb_4As_5)S_{17}$ [or $Tl_5(Sb,As)_{21}S_{34}$, as proposed by Shimizu *et al.* 1999]. The microprobe analysis and structural formula given by Nagl (1979) correspond to $x \sim 0$, and $y \sim 4.5$; it is close to chabournéite from Abuta. Similarly, the chabournéite-type compound from Hemlo (Harris 1989), with $x \sim –0.09$ and $y \sim 4.6$, is very close to Abuta chabournéite.

In dalnegroite, on the basis of $\Sigma Me = 13$ *apfu*, y varies between 5.77 and 6.02, with small variations of x. Its ideal structural formula is $[Tl_2PbSb]_{\Sigma4}\bullet(Sb_3As_6)S_{17}$. The unique analysis of "Pb-excess chabournéite derivative" from Abuta (Johan *et al.* 1981), has $x \sim 0.49$ and $y \sim 5.0$; this composition is close to $(Tl_{1.5}Pb_2Sb_{0.5})_{\Sigma4}\bullet(Sb_4As_5)S_{17}$ [or $Tl_3Pb_4(As,Sb)_{19}S_{34}$]. Such a Pb-excess derivative may correspond to a new member of the chabournéite series, but its crystal structure is unknown.

Table 10 reviews all the ideal structural formulae of members of the chabournéite series on the basis of the primitive cell (S = 17 atoms; $Z = 2$); these formulae are also marked in Figure 9. This figure, together with Table 9, shows that the members of the chabournéite series with $[Sb/(Sb + As)]_{at.}$ ratio close to 0.5, ranging from ~ 0.40 to 0.60, show superstructure reflections and non-centrosymmetric space group. On the other hand, protochabournéite, the only known member close to the Sb endmember, is centrosymmetric with a primitive and more regular unit cell. This absence of superstructure is clearly related to the high Sb content of protochabournéite, and not to the substitution $Sb^{3+} + Tl^+ \rightarrow 2\ Pb^{2+}$. In other words, a too low As content precludes As *versus* Sb partitioning and its consequences on the polymerization of $(Sb/As)S_3$ pyramids.

What is the exact definition of chabournéite?

The two chemical poles of the chabournéite solid solution, *i.e.*, "Pb-free" and "Pb-rich", correspond to the occupancy of the same position in the subcell by $(Tl_{0.5}Sb_{0.5})$ or Pb, respectively. This would correspond to two distinct mineral species. Unfortunately, the first definition of chabournéite (Mantienne 1974) is close to the "Pb-rich" pole, whereas the second, more accurate definition (Johan *et al.* 1981), corresponds to the "Pb-free" pole from the same deposit (Jas Roux).

Due to uncertainties about the exact crystal structure of chabournéite, it seems more appropriate to consider the "Pb-free" pole, with the simplest chemistry, as the ideal composition for chabournéite, that is $[Tl_2(Tl_{0.5}Sb_{0.5})Sb]_{\Sigma4}\bullet(Sb_4As_5)S_{17}$ or, on the basis of

TABLE 10. IDEAL STRUCTURAL FORMULAS IN THE CHABOURNÉITE SERIES RELATED TO VARIOUS MICROPROBE OR CRYSTAL STRUCTURE ANALYSES

Chemical pole	Ideal structural formula	Deposit
"Pb-free" chabournéite	$[Tl_2(Tl_{0.5}Sb_{0.5})Sb_1]_{\Sigma4}.(Sb_4As_5)S_{17}$	Jas Roux
"Pb-rich" chabournéite	$[Tl_2PbSb]_{\Sigma4}.(Sb_5As_4)S_{17}$	Jas Roux, Abuta, Hemlo
"Pb-excess chabournéite derivative"	$[Tl_{1.5}Pb_2Sb_{0.5}]_{\Sigma4}.(Sb_4As_5)S_{17}$	Abuta
Dalnegroite	$[Tl_2PbSb]_{\Sigma4}.(Sb_3As_6)S_{17}$	Binn
Protochabournéite	$[Tl_2PbSb]_{\Sigma4}.Sb_9S_{17}$	Monte Arsiccio

TABLE 11. SELECTION OF HOMEOTYPIC PAIRS AMONG SULFOSALTS RELATED TO THE PbS/SnS ARCHETYPES.

Homeotypic pair	Substitution rule	Crystallographic change	
		supercell/symmetry	Space group
pierrotite parapierrotite	As → Sb	2*a* – *b*, O – M	*Pna*2$_1$ - *Pn*
chabournéite protochabournéite	As → Sb	(2*a*, 2*b*) – (*a*, *c*)	*P*1 - *P*$\bar{1}$
edenharterite jentschite	As → Sb	(2*a*, 2*b*) - (*a*, *b*), O - M	*Fdd*2 - *P*2$_1$/*n*
guettardite twinnite	As → Sb	M - O	*P*2$_1$/*c* – *P*2$_1$/*n*
dufrénoysite rathite	2 Pb → As + Ag	No change	*P*2$_1$ - *P*2$_1$/*c*
quatrandorite senandorite	2 Pb → Sb + Ag	4*c* → 6*c*, M – O	*P*2$_1$/*c* - *Pn*2$_1$/*a*
aramayoite baumstarkite	Bi → Sb	No change	*P*1 - *P*$\bar{1}$
giessenite izoklakeite	Bi → Sb	M - O	*P*2$_1$/*n* - *Pnnm*
pavonite cupropavonite	y (Ag + Bi) → 3x Cu + 2x Pb	*c* → 2*c*	No change
makovickyite cupromakovickyite	(Ag, Bi) → (Cu, Pb)	*c* → 2*c*	No change
aikinite series	Bi → Pb + Cu	Various homeotypes	

Note: see Moëlo *et al*. (2008) for chemical formulas, and references therein for crystallographic data. Guettardite and twinnite: see Makovicky *et al*. (2012) and Makovicky & Topa (2012), respectively. Quatrandorite: see Nespolo *et al*. (2012).

S = 34 *apfu*, $Tl_5Sb_{11}As_{10}S_{34}$, in accordance with the simplified formula of Shimizu *et al*. (1999) and Moëlo *et al*. (2008).

Homeotype pairs among lead sulfosalts and related minerals

The chabournéite–protochabournéite couple is a new example in the vast group of sulfosalts related to the PbS or SnS archetypes where a small change in the chemistry, especially the Sb/As or Bi/Sb ratios, controls a crystallographic discontinuity between two close species, forming a homeotype pair. Table 11 lists various examples of such pairs, plus the complex aikinite homeotypic series, which contains eleven well-defined members. A crystal chemical trend can be seen in this list: when in a pair, the unit cell of one species is the supercell of the unit cell of the other ("superstructure effect"); this is related to a chemical substitution where a cation is replaced by a smaller cation (or a cation pair), with a more dissymmetric coordination [Sb → As, Ag → Cu, 2 Pb → (Sb,As) + Ag]. For the Sb-to-As substitution, this "superstructure effect" is directly related to the decrease in the size of polymeric $(Sb,As)_mS_n$ units, as pointed out by Doussier *et al*. (2008).

Summary and Conclusions

Protochabournéite is a new mineral species, the Sb-rich member of the chabournéite homeotypic series. It is close to $Tl_2PbSb_{10}S_{17}$, but this As-free member has not been discovered in nature up to now. So one can propose the formula ~ $Tl_2Pb(Sb_{9-8}As_{1-2})_{\Sigma 10}S_{17}$ as the simplified formula for protochabournéite. A crystal structure study permitted a general reexamination of the crystal chemistry of this series, and raised the question about the exact definition of chabournéite, taking into account the coexistence of Pb-free and Pb-excess varieties in the type deposit of Jas Roux.

Protochabournéite is the second new thallium sulfosalt discovered in the Monte Arsiccio mine. This fact, as well as other mineralogical and geochemical studies in progress, confirms the great complexity of the barite-pyrite-iron oxides ores in the Apuan Alps. Small changes in the complex ore composition in those deposits (and sometimes also within a single deposit), have led to the formation of a great variety of lead sulfosalts. The occurrence of a Sb-rich member of the chabournéite series is in agreement with the usual richness in Sb relative to As of the sulfosalts from the Apuan Alps district. For example, it is noteworthy that

Sb-rich phases related to baumhauerite, $Pb_5As_9S_{18}$, were discovered in these hydrothermal ores, namely boscardinite (Orlandi *et al*. 2012) and Sb-rich baumhauerite (Orlandi *et al*. 1996). In addition, routhierite from the Monte Arsiccio mine is enriched in antimony with respect to the occurrence at Jas Roux (Biagioni *et al*. submitted).

All occurrences of members of the chabournéite series (only five around the world) are typical of low temperature hydrothermal sulfide deposits, where the geochemical association of Pb, Tl, Sb, As, and some other metals (Cu, Zn, Hg, Ag…) controlled the formation of various sulfosalts. At Jas Roux, the type deposit of chabournéite (Mantienne 1974, Johan *et al*. 1981), the associated sulfosalts are pierrotite, parapierrotite, twinnite, zinkenite, "andorite", smithite, laffittite, and aktashite. This paragenesis is very similar to that of Monte Arsiccio. In the second chabournéite occurrence, the Toya-Takarada mine (Abuta-gun, Hokkaido, Japan; Johan *et al*. 1981, Shimizu *et al*. 1999), two other Tl-bearing sulfosalts are present: hutchinsonite and an unnamed mineral, $(Tl,Ag)_2Pb_6(As_{12}Sb_4)_{\Sigma 16}S_{31}$, which seems to be a Tl-rich derivative of baumhauerite-2*a*, ~ $Ag_{1.5}Pb_{22}As_{33.5}S_{72}$ (Pring *et al*. 1990). At Hemlo, chabournéite is associated with routhierite (Harris 1989).

In the Lengenbach quarry (Binntal, Switzerland), the type deposit of dalnegroite (Nestola *et al*. 2009), thirteen Tl-bearing species are present among numerous other sulfosalts: bernardite, edenharterite, erniggliite, gabrielite, hatchite, hutchinsonite, imhofite, jentschite, lorándite, rathite, sicherite, stalderite, and wallisite (Graeser *et al*. 2008).

Thus, the Monte Arsiccio deposit constitutes a new natural field of exploration for the crystal chemistry of thallium sulfosalts, as well as for the understanding of geological and geochemical processes which control the formation of thallium-rich sulfide ore deposits.

Acknowledgments

We are grateful to the mineral collector Riccardo Mazzanti for providing us with the first sample of protochabournéite. Electron microprobe analyses were performed with the help of O. Rouer (CNRS engineer, Institut des Sciences de la Terre d'Orléans). We are thankful to Georg Zagler who helped with the measurements of the reflectance spectra and the microhardness. Unpublished data for the unnamed chabournéite-type compound from Hemlo were communicated in the past (to Y.M.) by D. Harris. The suggestions of R. James Evans and an anonymous referee helped us in improving the paper.

References

Berlepsch, P., Armbruster, T., Makovicky, E., & Topa, D. (2003) Another step toward understanding the true nature of sartorite: Determination and refinement of a ninefold superstructure. *American Mineralogist* **88,** 450–461.

Bindi, L., Nestola, F., Guastoni, A., & Secco, L. (2010) The crystal structure of dalnegroite, $Tl_{5-x}Pb_{2x}(As,Sb)_{21-x}S_{34}$: a masterpiece of structural complexity. *Mineralogical Magazine* **74**, 999–1012.

Bonaccorsi, E., Biagioni, C., Moëlo, Y., & Orlandi, P. (2010) Chabournéite from Monte Arsiccio mine (Apuan Alps, Tuscany, Italy): occurrence and crystal structure. *20th General Meeting of the International Mineralogical Association (Budapest), Abstract Series* **6**, 714.

Brese, N.E. & O'Keeffe, M. (1991) Bond-valence parameters for solids. *Acta Crystallographica* **B47**, 192–197.

Carmignani, L., Dessau, G., & Duchi, G. (1972) I giacimenti minerari delle Alpi Apuane e loro correlazione con l'evoluzione del gruppo montuoso. *Memorie della Società Geologica Italiana* **11,** 417–431.

Carmignani, L., Dessau, G., & Duchi, G. (1976) I giacimenti a barite, pirite ed ossidi di ferro delle Alpi Apuane. Studio minerogenetico e strutturale. *Bollettino della Società Geologica Italiana* **95,** 1009–1061.

Costagliola, P., Benvenuti, M., Lattanzi, P., & Tanelli, G. (1990) The barite-pyrite-iron oxides deposit of Monte Arsiccio (Apuane Alps). Geological setting, mineralogy, fluid inclusions, stable isotopes and genesis. *Bollettino della Società Geologica Italiana* **109,** 267–277.

Del Bucchia, S., Jumas, J.C., & Maurin, M. (1981) Contribution à l'étude de composés sulfurés d'étain. (II). Affinement de la structure de SnS. *Acta Crystallographica* **B37,** 1903–1905.

Doussier, C., Moëlo, Y., Léone, P., Meerschaut, A., & Guillot-Deudon, C. (2008) Crystal structure of the new compound $Pb_{3+x}Sb_{3-x}S_{7-x}Cl_{1+x}$ ($x \sim 0.45$). The homologous series $Pb_{(2+2N)}(Sb,Pb)_{(2+2N)}S_{(2+2N)}(S,Cl)_{(4+2N)}Cl_N$ and its perchalcogenide derivative (N = 1 to 3). *Journal of Solid State Chemistry* **181,** 920–934.

Eisenmann, B. & Hofmann, A. (1991) Crystal structure of a calcium thioindate, $Ca_{0.76}In_{2.84}S_5$. *Zeitschrift für Kristallographie* **197,** 165–166.

Engel, P. (1980) Die Kristallstruktur von synthetischen Parapierrotit, $TlSb_5S_8$. *Zeitschrift für Kristallographie* **151,** 203–216.

Graeser, S., Cannon, R., Drechsler, E., Raber, T., & Roth, P., Eds. (2008) *Faszination Lengenbach. Abbau – Forschung – Mineralien 1958-2008*. Christian Weise Verlag, Munich, 192 pp.

HARRIS, D.C. (1989) The mineralogy and geochemistry of the Hemlo gold deposit, Ontario. *Geological Survey of Canada*, *Economic Geology Report* **38**.

JOHAN, Z., MANTIENNE, J., & PICOT, P. (1981) La chabournéite, un nouveau minéral thallifère. *Bulletin de Minéralogie* **104,** 10–15.

KRAUS, W. & NOLZE, G. (1996) POWDER CELL – a program for the representation and manipulation of crystal structures and calculation of the resulting X-ray powder patterns. *Journal of Applied Crystallography* **29,** 301–303.

LIMA-DE-FARIA, J., HELLNER, E., LIEBAU, F., MAKOVICKY, E., & PARTHÉ, E. (1990) Nomenclature of Inorganic Structure Types. Report of the International Union of Crystallography Commission on Crystallographic Nomenclature Subcommittee on the Nomenclature of Inorganic Structure Types. *Acta Crystallographica* **A46,** 1–11.

MAKOVICKY, E. (1985) The building principles and classification of sulphosalts based on SnS archetype. *Fortschritte der Mineralogie* **63,** 45–89.

MAKOVICKY, E. (1993) Rod-based sulphosalt structures derived from the SnS and PbS archetype. *European Journal of Mineralogy* **5,** 545–591.

MAKOVICKY, E. & TOPA, D. (2012) Twinnite, $Pb_{0.8}Tl_{0.1}Sb_{1.3}As_{0.8}S_4$, the OD character and the question of its polytypism. *Zeitschrift für Kristallographie* **227,** 468–475.

MAKOVICKY, E., TOPA, D., TAJJEDIN, H., RASTAD, E., & YAGHUBPUR, A. (2012) The crystal structure of guettardite, $PbAsSbS_4$, and the twinnite-guettardite problem. *Canadian Mineralogist* **50,** 253–265.

MANTIENNE, J. (1974) *La minéralisation thallifère de Jas Roux (Hautes-Alpes)*. Unpublished thesis, Université de Paris, 146 p.

MATSUSHITA, Y. & TAKÉUCHI, Y. (1994) Refinement of the crystal structure of hutchinsonite, $TlPbAs_5S_9$. *Zeitschrift für Kristallographie* **209**, 475–478.

MOËLO, Y., GUILLOT-DEUDON, C., EVAIN, M., ORLANDI, P., & BIAGIONI, C. (2012) Comparative modular analysis of two complex sulfosalt structures: sterryite, ~$Cu(Ag,Cu)_3Pb_{19}(Sb,As)_{22}(As\text{-}As)S_{56}$, and parasterryite, $Ag_4Pb_{20}(Sb,As)_{24}S_{58}$. *Acta Crystallographica* **B68,** 480–492.

MOËLO, Y., ORLANDI, P., GUILLOT-DEUDON, C., BIAGIONI, C., PAAR, W., & EVAIN, M. (2011) Lead-antimony sulfosalts from Tuscany (Italy). XI. The new mineral species parasterryite, $Ag_4Pb_{20}(Sb_{14.5}As_{9.5})_{\Sigma 24}S_{58}$, and associated sterryite, $Cu(Ag,Cu)_3Pb_{19}(Sb,As)_{22}(As\text{-}As)S_{56}$, from the Pollone mine, Tuscany, Italy. *Canadian Mineralogist* **49,** 623–638.

MOËLO, Y., MAKOVICKY, E., MOZGOVA, N.N., JAMBOR, J.L., COOK, N., PRING., A., PAAR, W.H., NICKEL, E.H., GRAESER, S., KARUP-MØLLER, S., BALIC-ŽUNIC, T., MUMME, W.G., VURRO, F., TOPA, D., BINDI, L., BENTE, K., & SHIMIZU, M. (2008) Sulfosalt systematics: a review. Report of the sulfosalt sub-committee of the IMA Commission on Ore Mineralogy. *European Journal of Mineralogy* **20,** 7–46.

NAGL, A. (1979) The crystal structure of a thallium sulfosalt, $Tl_8Pb_4Sb_{21}As_{19}S_{68}$. *Zeitschrift für Kristallographie* **150,** 85–106.

NESPOLO, M., OZAWA, T., KAWASAKI, Y., & SUGIYAMA, K. (2012) Structural relations and pseudosymmetries in the andorite homologous series. *Journal of Mineralogical and Petrological Sciences* **107,** 226–243.

NESTOLA, F., GUASTONI, A., BINDI, L., & SECCO, L. (2009) Dalnegroite, $Tl_{5-x}Pb_{2x}(As,Sb)_{21-x}S_{34}$, a new thallium sulphosalt from Lengenbach quarry, Binntal, Switzerland. *Mineralogical Magazine* **73,** 1027–1032.

ORLANDI, P., DEL CHIARO, L., & PAGANO, R. (1996) Minerals of the Seravezza Marble, Tuscany, Italy. *Mineralogical Record* **27,** 47–58.

ORLANDI, P., MOËLO, Y., MEERSCHAUT, A., & PALVADEAU, P. (1999) Lead-antimony sulfosalts from Tuscany (Italy): I. Scainiite, $Pb_{14}Sb_{30}S_{54}O_5$, the first Pb-Sb oxy-sulfosalt, from Buca della Vena mine. *European Journal of Mineralogy* **11,** 949–954.

ORLANDI, P., MOËLO, Y., MEERSCHAUT, A., & PALVADEAU, P. (2001) Lead-antimony sulfosalts from Tuscany (Italy): III. Pillaite, $Pb_9Sb_{10}S_{23}ClO_{0.5}$, a new Pb-Sb chloro-sulfosalt, from Buca della Vena mine. *European Journal of Mineralogy* **13,** 605–610.

ORLANDI, P., BIAGIONI, C., BONACCORSI, E., MOËLO, Y., & PAAR, W. (2012) Lead-antimony sulfosalts from Tuscany (Italy): XII. Boscardinite, $TlPb_4(Sb_7As_2)_{\Sigma 9}S_{18}$, a new mineral species from the Monte Arsiccio mine: occurrence and crystal structure. *Canadian Mineralogist* **50,** 235–251.

ORLANDI, P., MOËLO, Y., MEERSCHAUT, A., PALVADEAU, P., & LÉONE, P. (2004) Lead-antimony sulfosalts from Tuscany (Italy): VI. Pellouxite, ~ $(Cu,Ag)_2Pb_{21}Sb_{23}S_{55}ClO$, a new oxy-chloro-sulfosalt, from Buca della Vena mine. *European Journal of Mineralogy* **16,** 839–844.

ORLANDI, P., MOËLO, Y., MEERSCHAUT, A., PALVADEAU, P., & LÉONE, P. (2005) Lead-antimony sulfosalts from Tuscany (Italy): VIII. Rouxelite, $Cu_2HgPb_{22}Sb_{28}S_{64}(O,S)_2$, a new sulfosalt from Buca della Vena mine, Apuan Alps: definition and crystal structure. *Canadian Mineralogist* **43,** 919–933.

OTWINOWSKI, Z. & MINOR, W. (1997) Processing of X-ray diffraction data collected in oscillation mode. *In* Methods in Enzymology: Macromolecular Crystallography (C.W. Carter, Jr. & R.M. Sweet, eds.). Academic Press, New York, U.S.A. (307–326).

PANDELI, E., BAGNOLI, P., & NEGRI, M. (2004) The Fornovolasco schists of the Apuan Alps (Northern Tuscany, Italy): a new hypothesis for their stratigraphic setting. *Bollettino della Società Geologica Italiana* **123,** 53–66.

PRING, A., BIRCH, W.D., SEWELL, D., GRAESER, S., EDENHARTER, A., & CRIDDLE, A. (1990) Baumhauerite-2*a*: a silver-bearing minerals with a baumhauerite-like supercell from Lengenbach, Switzerland. *American Mineralogist* **75,** 915–922.

SHELDRICK, G.M. (2008) A short history of SHELX. *Acta Crystallographica* **A64**, 112–122.

SHIMIZU, M., MATSUYAMA, F., & SHIMIZU, M. (1999) Hutchinsonite, $TlPb(As,Sb)_5S_9$, Chabournéite, $Tl_2Pb(Sb,As)_{10}S_{17}$, and Unnamed $(Tl,Ag)_2Pb_6(As,Sb)_{16}S_{31}$ from the Toya-Takarada Mine, Hokkaido, Japan – Tl mineralisation in the Kuroko Deposits. *Resource Geology* **20,** 31–37.

Received June 14, 2012, revised manuscript accepted May 12, 2013.